

# Spiral waves in accretion discs - observations

Danny Steeghs

Physics & Astronomy, Southampton University, Southampton SO17 1BJ, UK

**Abstract.** I review the observational evidence for spiral structure in the accretion discs of cataclysmic variables (CVs). Doppler tomography is ideally suited to resolve and map such co-rotating patterns and allows a straightforward comparison with theory. The dwarf nova IP Pegasi presents the best studied case, carrying two spiral arms in a wide range of emission lines throughout its outbursts. Both arms appear at the locations where tidally driven spiral waves are expected, with the arm closest to the gas stream weaker in the lines compared to the arm closest to the companion. Eclipse data indicates sub-Keplerian velocities in the outer disc. The dramatic disc structure changes in dwarf novae on timescales of days to weeks, provide unique opportunities for our understanding of angular momentum transport and the role of density waves on the structure of accretion discs. I present an extension to the Doppler tomography technique that relaxes one of the basic assumptions of tomography, and is able to map modulated emission sources. This extension allows us to fit anisotropic emission from, for example, spiral shocks, the irradiated companion star and disc-stream interaction sites.

## 1 Accretion discs and angular momentum

The energetic phenomena associated with a wide range of accreting systems rely on the efficient conversion of potential energy into radiation and heat. In close binaries, the deep potential well of the compact object leads to mass transfer and accretion once the companion star evolves and Roche lobe overflow commences. The efficiency of accretion is proportional to the compactness,  $M/R$ , of the accreting compact star with mass  $M$  and radius  $R$ . As matter spills over near the first Lagrangian point, it sets off on a ballistic trajectory towards the accretor. Its potential energy is converted into kinetic energy, but its net angular momentum, due to orbital motion of the mass donor, prevents a straightforward path to the accretor. The natural orbit for such matter is a circular Keplerian orbit corresponding to its specific angular momentum. Instead of dumping material directly onto the compact star, the primary Roche lobe is slowly filled with a near Keplerian disc. Angular momentum needs to be dispersed within this accretion disc in order to allow gas to spiral inwards towards the compact star [7].

It is the detailed process of angular momentum transport that determines the structure of this accretion disc and therefore the rate at which gas, supplied from the mass donor, is actually accreted by the compact object. Although so fundamental to the process of accretion through discs, our understanding of angular momentum dispersal is very limited. We can roughly divide the possible physical

mechanisms that may provide the required angular momentum transport into two classes. Those that work on a local scale and exchange angular momentum among neighbouring parcels in the disc, and those that rely on global, large scale structures in the disc. The local processes are commonly referred to as ‘viscous processes’ even though it was clear that the molecular viscosity of the accretion disc material itself was many orders of magnitudes too small [14]. Viscous interaction in the sheared Keplerian disc allows some material to spiral inwards, losing angular momentum, while excess momentum is carried outwards by other parts of the flow. In the famous  $\alpha$ -parameterisation of Shakura & Sunyaev [22], this viscosity was replaced by a single dimensionless constant, which allows one to solve the structure equations for thin, viscously heated accretion discs [19].

A very different way of transporting the angular momentum is via density waves in the disc. In self-gravitating discs, the ability of density waves to transport angular momentum is a direct result from purely gravitational interaction between the wave and the surrounding disc material [31,4]. Waves of this type can still transport angular momentum in the absence of self gravity, provided some mechanism exists that exchanges momentum between the wave and the fluid. Sawada et al. [21] conducted numerical simulations of mass transfer via Roche lobe overflow of inviscid, non self gravitating discs, and witnessed the development of strong spiral shocks in the disc which were responsible for the bulk of the angular momentum transport throughout the flow. Such trailing spiral patterns are the natural result of a tidal deformation of the disc that is sheared into a spiral pattern by the (near) Keplerian rotation profile of the disc material [20].

In this review I aim to give an overview of the observational efforts to study such spiral structures in the discs of cataclysmic variables (CVs). Tomography is ideally suited for the study of disc structure, and the detection of a spiral structure in the disc of IP Pegasi [27], 13 years after the work by Sawada et al., triggered a renewed interest in such models. Boffin, this volume, will focus on the theoretical side of the issue and the comparison between the observations and numerical simulations of spiral waves in discs.

## 2 Prospect for detecting spiral waves in discs

Tidally generated spiral waves are the result of tidal torques of the companion star on the orbiting disc material. Initially triggered at the outer edge of the disc, where the tidal interaction between the disc and the companion star is strongest, they take the form of trailing spirals because the azimuthal velocity of the disc material is supersonic and increases monotonically with decreasing distance from the compact object ( $v_\phi \propto r^{-1/2}$ ). Both the density as well as the disc temperature are much higher at the location of the spirals, and continuum and line emission from such spirals can thus be expected to be in clear contrast with the surrounding areas of the disc. This contrast depends on the density contrast in the wave, i.e. the strength of the shock, as well as local radiative transfer conditions.

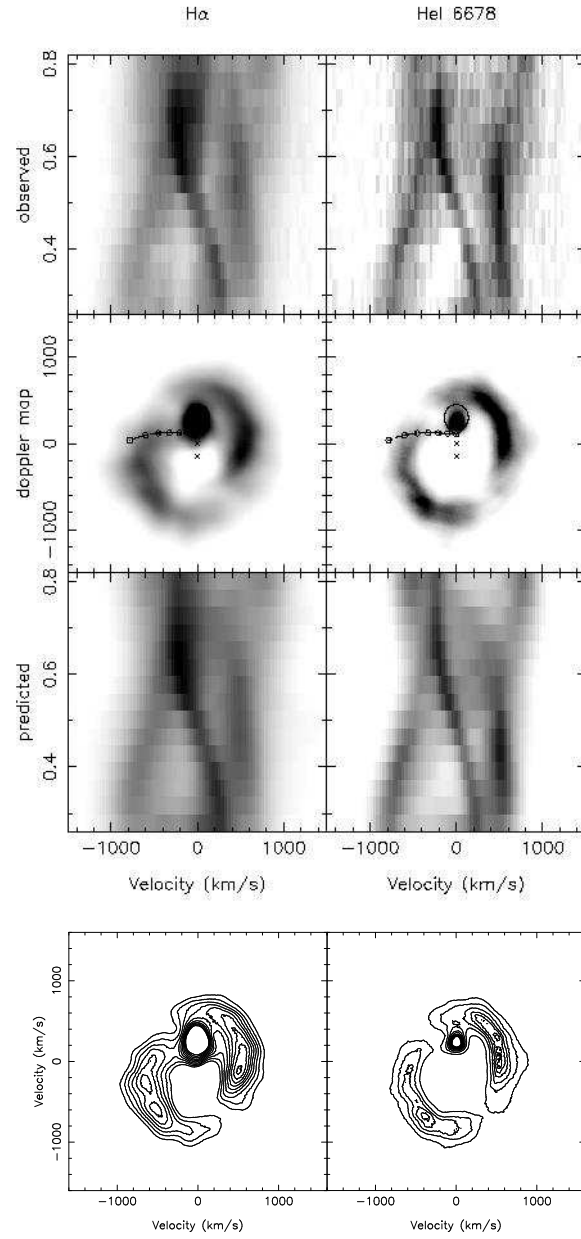


**Fig. 1.** Top; the observed  $H\alpha$  and HeI emission line profiles during the early stages of an IP Pegasi outburst. The maximum entropy Doppler tomograms (second row) reveal a prominent spiral pattern in the disc as well as secondary star emission. Third row of panels are the predicted line profiles given the calculated maps. Bottom row is a contour plot of the Doppler tomograms. From [27].

Although predicted in the 80s, observational evidence for spirals relies on the ability to spatially resolve the accretion discs in interacting binaries. Indirect imaging methods are thus required to search for such global disc asymmetries. Since the wave pattern is a co-rotating structure close to the orbital plane, Doppler tomography of strong emission lines is the ideal tool at hand. Although providing an image of the line emission distribution in velocity space, and not spatial coordinates, spirals should be readily identified as they maintain their spiral shape in the velocity coordinate frame.

Since the application of Doppler tomography to the discs in CVs (Marsh, this volume), a range of objects have been imaged, showing a rich variety of accretion structures, but no clear evidence for spiral arms in the accretion discs. This was part of the reason that the interest in spiral waves diminished after a series of landmark papers in the late eighties [23,24], and a solution to the angular momentum puzzle was sought in local magneto-turbulent processes [1]. In 1997, however, convincing observational evidence for tidally driven spirals in the disc of a CV was found for the first time.

### 3 IP Pegasi in outburst

As part of a programme to study the disc evolution of the dwarf nova IP Pegasi through Doppler tomography, the system was observed just after rise to one of its outbursts. Although such outbursts occur regularly and have a characteristic recurrence time, one cannot predict them accurately. Obtaining scheduled telescope time during such outbursts is therefore not straightforward. For IP Pegasi, the average recurrence time for outbursts is 88 days, with a considerable RMS variation of 18 days [25].

When a Doppler map was constructed of the hydrogen and helium emission from IP Pegasi, a surprising emission pattern was found [27,28]. The accretion disc was far from symmetric, instead disc emission was dominated by a two armed pattern in the lower left and upper right quadrants of the Doppler map (Figure 1). The spiral arm velocities range between 500 and 700 km/s, corresponding to the outer regions of the accretion disc. The emissivity contrast between the spirals and other parts of the disc, is about a factor of  $\sim 3$  for  $H\alpha$ , and  $\sim 5$  in the case of  $HeI6678$  emission. There is no evidence for line emission from the bright spot. The spiral arm in the lower quadrant, closest to the secondary, extends over an angle of  $\sim 100^\circ$ , and is weaker than the arm in the opposite quadrant. Strong emission from the irradiated secondary star is also present, producing the prominent S-wave at low velocities.

The location of this pattern corresponds closely to the radii and azimuths where tidally driven spiral waves are expected. Although the Doppler map is in velocity coordinates, and not Cartesian position coordinates, a spiral pattern in position space corresponds to a spiral pattern in velocity space. In Figure 2, a simple disc model is shown containing an accretion disc around the white dwarf with a purely geometrical spiral pattern and a Keplerian velocity field. The two armed trailing spiral in position coordinates, maps into a similar two armed

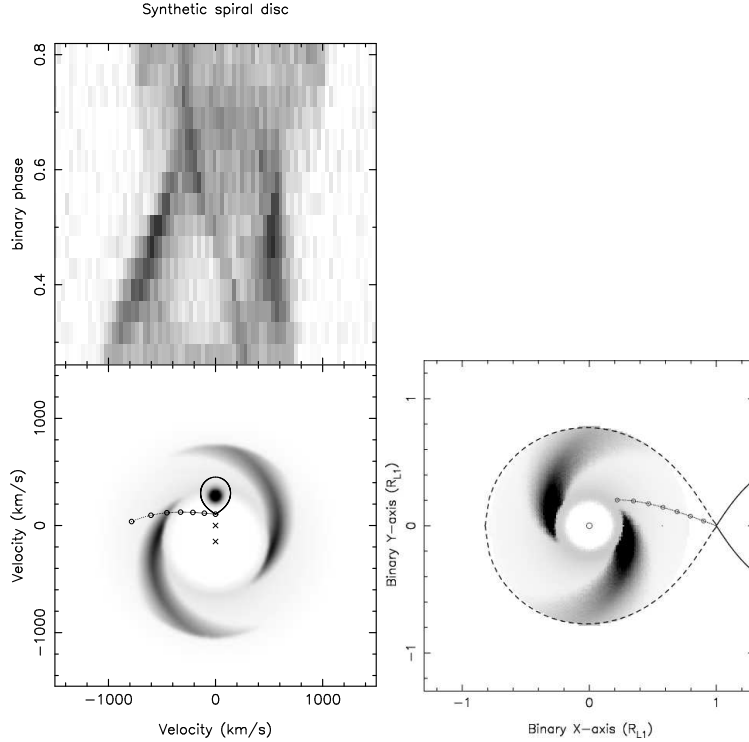


**Fig. 2.** A simple model of a disc carrying a two armed spiral pattern. Bottom right the distribution of emission in XY coordinates, bottom left in Doppler coordinates and top is the predicted line profiles from such a disc. From [27]

pattern in velocity space. Although this model is a purely geometric pattern, the location of the spiral roughly corresponds to the location in the disc where tidally driven waves are expected from model simulations. Even such a simple model already captures most of the structure we observe in IP Pegasi, indicating that most of the disc emission in IP Peg during outburst is indeed localised in a two armed pattern.

Let us look at the main signatures of spiral arms in the observable line profiles based on our simple model. In Figure 3, the velocity and emissivity of the model disc is plotted as a function of azimuth in the Doppler tomogram. Azimuth 0 corresponding to the positive  $V_y$  axis, increasing clockwise. The defining feature of a trailing spiral is the change in velocity as a function of azimuth in the tomogram. This corresponds to a change in radius  $R$  as a function of azimuth  $\theta$  in position coordinates that is determined by the opening angle of the spiral,  $dR/d\theta$ . The velocity field of the disc relates this geometrical opening angle to a particular velocity-azimuth relation in the Doppler map. In the spiral arm dominated line profiles, this produces a regular motion of the double peaks, since azimuth in position coordinates translates to orbital phase in the observed spectrogram.

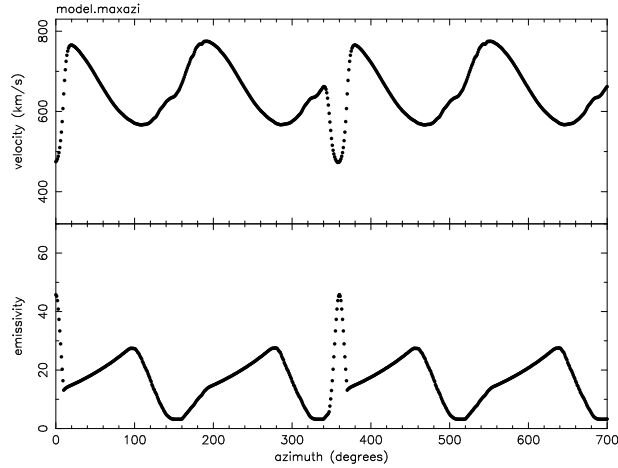


**Fig. 3.** The azimuthal dependence of a two armed spiral produces a periodic variation in the velocity and emission strength of the spiral as a function of azimuth. The features near azimuth zero are due to the presence of companion star emission, which is also present in the observed data.

Near orbital phases 0.25 and 0.75, the two arms cross over, producing a sudden jump in the position of the double peaks. For a symmetric Keplerian disc on the other hand, the line profile is symmetric and the velocity of the double peaks correspond to the velocity of the outer edge of the disc. This results in a constant double peak separation as a function of orbital phase and a circular disc image in the Doppler map. With a two armed spiral, the double peaks move, varying their separation considerably and sharply across the binary orbit in a particular way. Although an identification in Doppler maps is perhaps more straightforward, spirals may thus also be identified in the observed line profiles directly.

A week later, during the same outburst, more spectroscopy was obtained before the decline of the outburst had started. The Doppler image (Figure 4) shows that the spiral pattern persists throughout the outburst, and the secondary star now makes a considerably larger contribution (from 6% to 10%) to the line flux. The arm in the upper right quadrant is still stronger, and the location of the arms have not changed, although the upper right arm appears shorter. To highlight the spiral arms in the line profiles, the S-wave of the secondary star was subtracted from the data in the following manner. A Roche lobe shaped mask was used to select all the emission from the secondary, which was then projected in order to produce the trailed spectrogram of the red star emission. This was subtracted from the observed data, and a Doppler image of the disc emission only was constructed (Figure 4, right). The dramatic phase dependence of the double peaks is now clearly visible, and is directly related to the two spiral arms in the disc. This also confirms that the presence of a strong S-wave due to the mass donor does not distort the reconstructed disc structure, since they occupy different locations in the velocity plane.

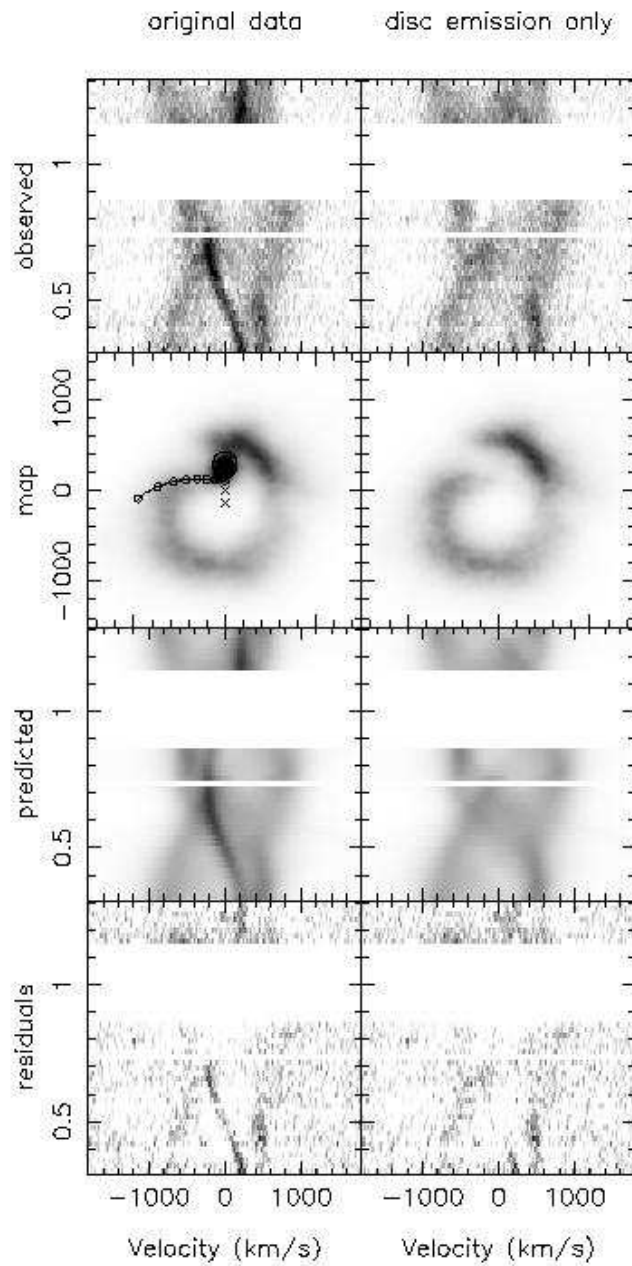


**Fig. 4.** The spiral pattern persists throughout the outburst, above are HeI6678 data towards the end phases of outburst maximum. From top to bottom, observed data, Doppler map, predicted data and residuals. For the right hand panels, the contribution from the secondary star has been subtracted. From [25]

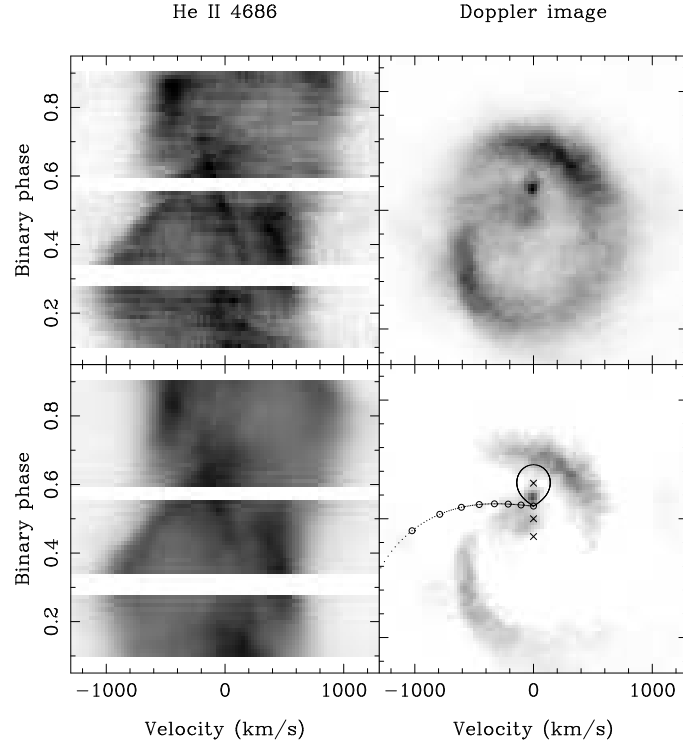


**Fig. 5.** Ionised helium from the disc in IP Pegasi during the November 1996 outburst. The familiar spiral arms are present also in this line, together with emission from the front side of the secondary. Subtracting the symmetric component from the Doppler map, highlights the two armed spiral (bottom). Observed and predicted data are in the top left and bottom left panel respectively.

### 3.1 Ionised Helium from the disc

In a different outburst Harlaftis et al. [11] secured a whole orbit, including eclipse, of IP Pegasi with high spectral (40 km/s) and phase resolution (0.01). This time, the outburst started two days before the observations, and the HeII emission line at  $4686\text{\AA}$  was observed to provide a comparison with the previously observed  $H\alpha$  and HeI emission patterns. The trailed spectrogram of HeII (Figure 5), again shows the familiar behaviour of the double peaks from the disc, leading to a two armed spiral in the Doppler tomogram. A very similar emission pattern from the disc was also present in the nearby Bowen blend consisting of CIII/NIII emission and the Helium I line at  $4471\text{\AA}$ . The symmetric component of the map was calculated, using the velocity of the white dwarf as the centre of symmetry, and subtracted in order to highlight the location of the two arms (Figure 5, bottom right).

In order to characterise the properties of the spirals quantitatively, we determined the position of the two spiral arms as a function of velocity in the re-



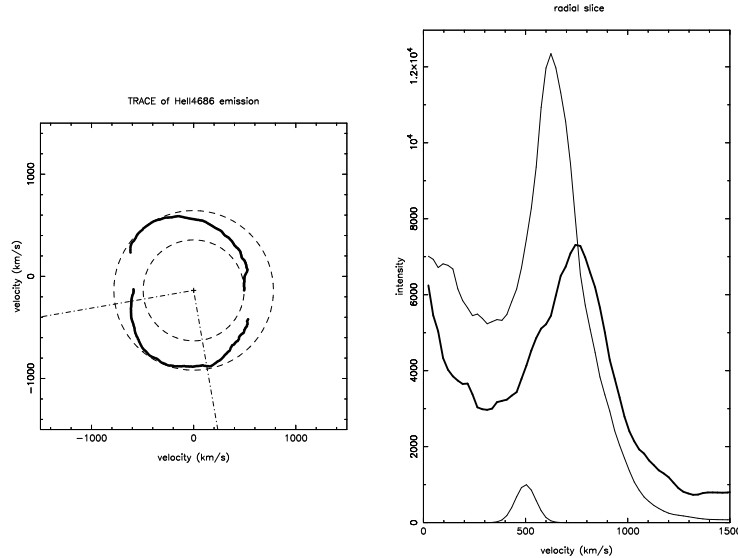


**Fig. 6.** Tracing the spiral arms in the Doppler map through cross correlation with a Gaussian. Two radial slices through the Doppler map are plotted in the right panel, revealing the radial extent and position of the spiral arms. The instrumental profile (lowest curve) is plotted for comparison. The fitted positions of the spiral arms in the velocity plane are shown in the left panel. Circles denote the maximum/minimum velocity of the spirals and the two lines indicate the azimuth of the two slices plotted on the right.

constructed tomogram. A slice through the map, starting from the white dwarf at  $V_y = -137$  km/s, was made for each azimuth in order to extract the radial profile. Each radial profile was then cross correlated with a Gaussian in order to determine the velocity of the spiral at that particular azimuth. Figure 6 plots the fitted positions of the spirals in the velocity plane together with two radial slices across the map. The two spirals can be traced for almost 180 degrees, and the velocity of the arms varies from 495 km/s to 780 km/s, indicated by the two dashed circles. Near the azimuths where the spiral cross over, the fitting assumptions break down as there is a sudden transition between the velocity of one arm and the next. Unfortunately, the contrast of the arms is too low to follow this switching with our cross correlation method, or a double Gaussian. The widths of the arms are significant, and even change as a function of azimuth. We are thus resolving an intrinsically broad feature. Such an analysis will clearly profit from even higher resolution and signal to noise data since at peak intensity the width of the arm is comparable to our resolution element, and the maximum entropy constraint will tend to broaden features as much as is allowed by the signal to noise of the data.

A tidally distorted disc will not have a pure Keplerian velocity field, and we will see later that the observations indeed indicate this is not the case in IP Pegasi. However, we can estimate the radii corresponding to the velocity of

the spirals under the assumption of Keplerian velocities. The arms then cover a substantial part of the disc, between 0.3 and 0.9 times the distance to the  $L_1$  point, with the strongest emission from the outer regions. The dynamics of the majority of the accretion disc material are thus affected by the presence of these spirals.

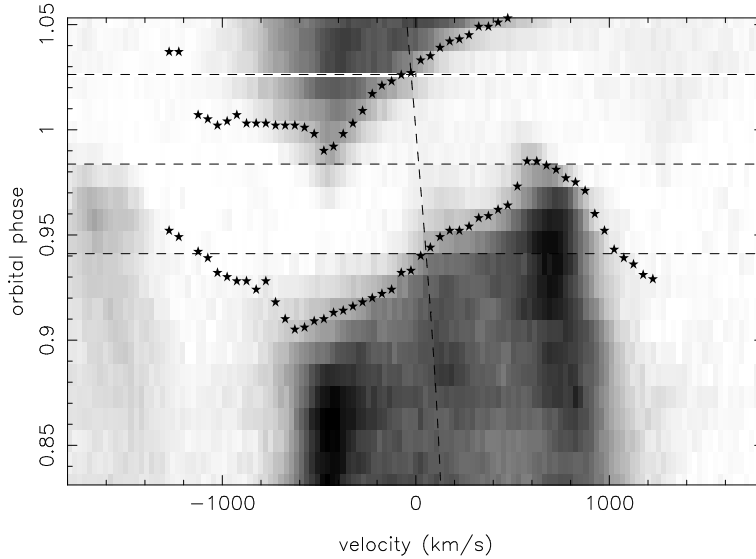


**Fig. 7.** Measurements of the phases of half depth across the HeII eclipse are denoted by asterisks. Horizontal, dashed lines are the average post-eclipse half depth (top), pre-eclipse half-depth (bottom) and mid-eclipse. The orbital phases are based on the conjunction of the white dwarf.

The eclipses of the lines are also affected by the large accretion disc asymmetry. In Figure 7, the eclipse of the Helium II emission line is plotted. For each velocity bin, the orbital phases where half the light is eclipsed are marked by asterisks. The outer disc on the blue-shifted peak is eclipsed first, followed by emission at higher, blue-shifted velocities. After the blue side of the disc is covered, the red-shifted emission is progressively eclipsed, and during egress, the situation reverses. This is the classical pattern of the eclipse of a pro-gradely rotating disc, where the disc velocity increases with decreasing radius. A strictly Keplerian accretion disc would result in a smooth eclipse, symmetric around orbital phase 0. Mid-eclipse for the disc emission from IP Peg occurs considerably earlier (orbital phase 0.987) compared to the continuum, and most of the light is eclipsed well before white dwarf ingress. A large asymmetry in the outer disc is thus corroborated by the eclipse. The distorted disc eclipse is a combination of the spiral asymmetry as well as deviations from Keplerian velocities. Although these eclipse phases are not fitted by Doppler tomography codes, high quality

eclipse data has the potential to reveal departures from Keplerian velocities and disentangle these two effects.

Eclipse mapping of this data in both the lines and continuum, reveals the presence of a two armed asymmetry in the outer regions of the disc, at the azimuths corresponding to the spiral arms in the Doppler maps [2] (see also Baptista, this volume). The velocities of the spirals as derived from the emission lines, can be compared with the position of the spirals from the eclipse map. This indicates that velocities near the spirals deviate considerably from the local Keplerian value. The two imaging methods thus nicely complement each other and both support a tidal interpretation of the spirals.

Apart from the data sets discussed here, Morales-Rueda et al. [18], also recovered prominent spiral waves in the disc of IP Pegasi during outburst in a range of emission lines. The disc structure during their observations, about 5 days after the start of the outburst, is very similar to the Doppler maps presented here, with a slightly stronger arm in the upper right quadrant. They also note the shifted emission line eclipses and shielding of the irradiated companion star by the geometrically thick disc.

Doppler tomography of IP Pegasi during outburst thus invariably shows the presence of spiral shaped disc asymmetries. The two armed spiral dominates the disc emission from the start of the outburst maximum and persists for at least 8 days, corresponding to about 50 binary orbits. The spirals are present in a range of emission lines from neutral hydrogen to ionised helium, the latter indicating that the gas concerned has to be hot, although it is not clear if we are looking at direct emission from the shock, or recombination emission from the spiral arms. The asymmetry between the two arms that was observed in the discovery data, is also present at other epochs and in other lines. The disc structure is co-rotating with the binary, and corresponds to the velocities were tidally driven spiral arms are expected. A more detailed comparison between theory and observations is discussed by Boffin, this volume. We shall see that the observed properties of the spirals fit recent hydro-dynamical simulations of such discs in detail [26].

Although the disc emission of the different data sets is in general terms the same, differences between the various data sets should tell us something about the evolution of the spiral across the outburst (and therefore their origin). In addition, comparing lines with different excitation potential allows us to investigate the physical conditions of the emitting gas directly. Unfortunately, the various data sets have been obtained with different telescopes and instruments, different resolutions, and different orbital phase coverage. Disentangling those systematic effects from true variations of the spiral in various lines is therefore not straightforward. Ideally one would observe a range of emission lines simultaneously with the same instrumental setup, while covering a substantial part of the disc outburst to study its evolution. As a first step, we have obtained echelle spectroscopy of IP Pegasi during a recent outburst with the NTT (Steeeghs & Boffin, in preparation). Covering a large part of the optical spectrum at high resolution, ensures that we will be able to compare the properties of the spiral among a large set of emission lines, obtained under identical circumstances. Fig-

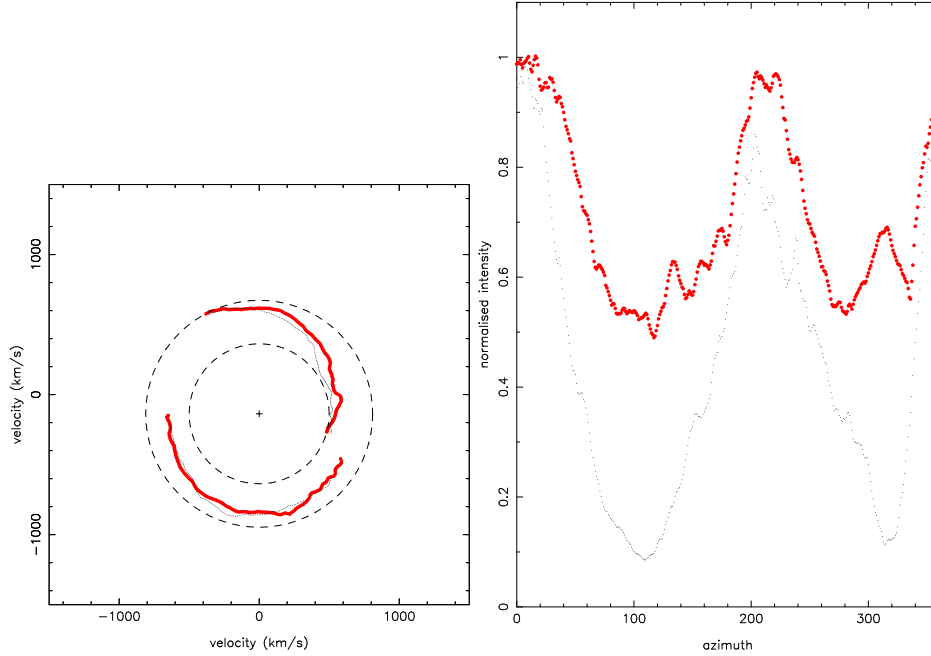


**Fig. 8.** Comparing the properties of the spirals in two emission lines from the same data set. The position and intensity of the spirals were traced as a function of azimuth in the  $H\alpha$  (thick line) and  $HeI6678\text{\AA}$  tomograms constructed from NTT echelle spectroscopy during the August 1999 outburst of IP Peg. The intensities are normalised with respect to the maximum emissivity values of each line.

ure 8 compares the properties of the spirals between just two lines covered, and indicates a very similar position for the spirals in terms of velocity as a function of azimuth for the  $H\alpha$  and  $HeI6678\text{\AA}$  lines. The intensity modulation, on the other hand is significantly different.

#### 4 The quiescent disc

In stark contrast with the prominent spiral waves observed during outburst, Doppler mapping of IP Pegasi during quiescent epochs does not reveal such features [15,13,10,33]. Although significant disc asymmetries are observed even during quiescence, it is clear that the open spiral pattern the disc carries in outburst is not present. The disc radii of dwarf novae are expected to vary significantly across the outburst cycle. In the disc instability picture, a dwarf nova disc is in a cool state during quiescent phases, when most mass transferred from the mass donor is not accreted by the white dwarf. The disc density builds up until a radical opacity change due to the ionisation of hydrogen flips the disc from a neutral, cool state to a hot, ionized state. Angular momentum transport in this hot state is increased by a factor of 10 or so, which results in a rapid

expansion of the disc at the onset of the outburst. During outburst, the disc is depleted as more mass is accreted than is transferred from the mass donor, until the density in the disc drops below the critical value again and the system returns to quiescence.

Disc radius variations are indeed observed in dwarf novae, and the disc in IP Pegasi fills between half of the primary Roche lobe during quiescence up to most of the Roche lobe during outburst [34,32,25]. Tidally driven waves are thus much more likely to have an effect on the disc in outburst, since the tidal torques are a steep function of the distance to the secondary star. The fact that spirals are not prominent in quiescence, is therefore what one expects if they are due to the tidal torques of the companion star [26]. The detailed properties of the spirals depend upon disc temperature, radius and the mass ratio of the binary. The most likely discs carrying prominent open-armed spirals are thus dwarf novae in outburst and the nova-like variables, where the disc is always in the hot, ionised state. Dwarf novae are likely to display highly variable spiral arm structures, depending on the state of the system, whereas nova-like variables would provide a more persistent tidal pattern since large disc radius variations are relatively rare.

Marsh, this volume, has compiled an up to date overview of all the systems for which Doppler maps have been published. One would perhaps expect that such spirals should have been found before if they are a common phenomenon. The number of Doppler maps of dwarf novae in outburst are very rare indeed. And even in quiescence, some well known systems have not yet been mapped using good quality data. Unfortunately, in the case of nova-likes where one would have the potential of observing a persistent spiral pattern, Doppler mapping has shown complicated emission geometries. In those systems, line emission is not dominated by a disc component, instead prominent spots dominate the tomograms whose interpretation is unclear. However, IP Pegasi is no longer the only system with evidence for distortions of a spiral nature. The next section will discuss a small number of other systems which display very similar disc behaviour.

## 5 Disc asymmetries in other systems

### 5.1 EX Dra

The dwarf nova EX Dra was the second object to show similar disc behaviour. This is another eclipsing system above the period gap and is in many ways very similar to IP Pegasi [3,6]. Joergens et al. [12] present Doppler images of EX Dra during outburst, and the similarity of the Doppler maps with those of IP Pegasi is obvious (Figure 9). Although perhaps not as convincing as in IP Pegasi in all the mapped lines, the disc carries a two armed asymmetry during outburst in the same quadrants of the Doppler map. The appealing characteristic of this object is its very short outburst recurrence time. Although its orbital period and mass ratio is very similar to IP Peg, EX Dra's outbursts recur every 23 days, and catching such a system in outburst is thus more likely. It would be an ideal

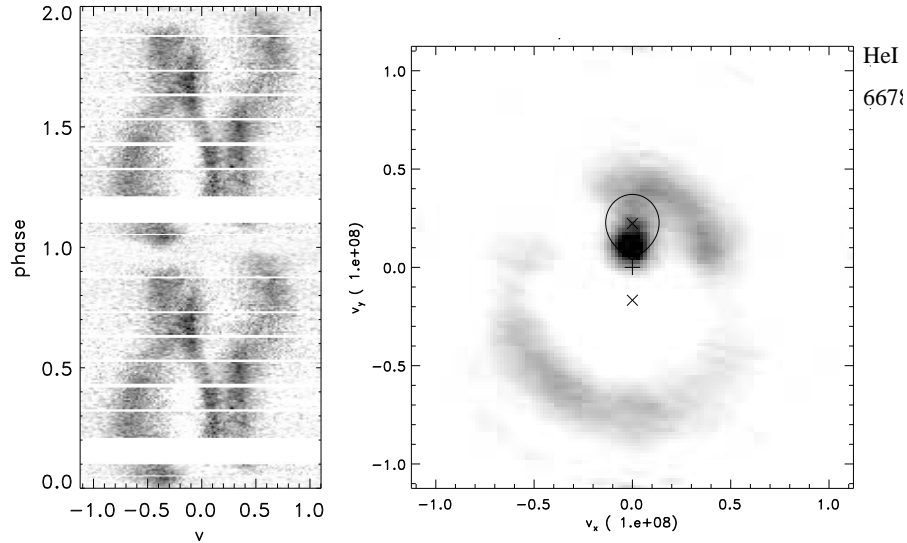


**Fig. 9.** Doppler tomography of EX Dra in outburst [12]. Left the observed HeI 6678Å emission and its tomogram on the right. Apart from the irradiated secondary, the disc contains a two armed asymmetry with a shorter arm in the top right and a more extended arm in the lower left quadrant.

target for a longer campaign, with the prospect of securing the disc evolution across the whole outburst cycle, and performing time lapsed tomography in order to construct a movie of the accretion disc along its outburst cycle. A photometric campaign lasting over 6 weeks was conducted during the summer of 2000, just after this workshop. Although no Doppler tomography will be possible, two outburst cycles were covered, and eclipse mapping methods will reveal the development of disc asymmetries and radial temperature variations.

## 5.2 U Gem

U Gem is one of the brightest and best studied CVs, reaching a magnitude of  $V \sim 8.5$  during outburst. Surprisingly, no outburst Doppler tomography of this system was available until very recently, Groot observed the system during the March 2000 outburst [8]. Figure 10 shows the HeII tomogram of U Gem in outburst, revealing a prominent two armed spiral pattern. The spirals are strong even towards the late phases of the outburst maximum, and weaken once decline sets in. This supports a tidal interpretation for these structures since the spirals are there when the disc is hot and large, but weaken once the disc shrinks back towards quiescence like in IP Pegasi. The rise and decline phases of the outbursts are particularly useful for testing the tidal interpretation of spiral waves. During those phases the spiral arm geometry will change dramatically, and the exact nature of the evolution will tell us if indeed the spirals behave as tidally driven

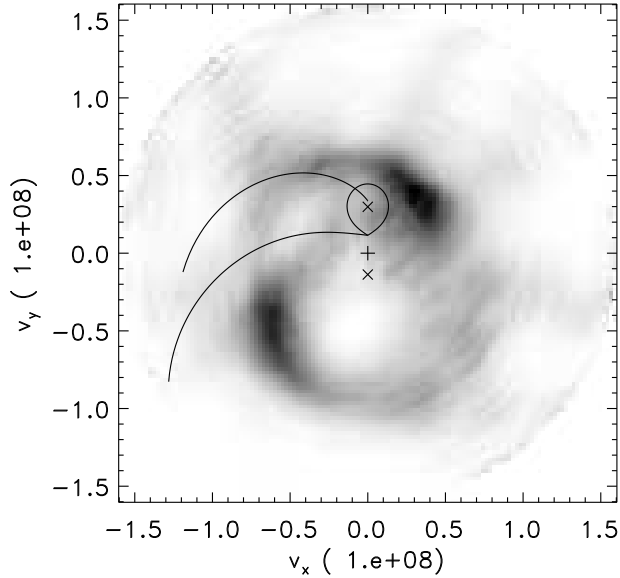


**Fig. 10.** Doppler tomogram of the HeII 4686Å emission from U Gem in outburst [8]. Two striking spiral arms are revealed, matching the properties of a tidal spiral pattern.

spirals would do, and how they affect the angular momentum exchange in the accretion disc.

### 5.3 SS Cyg

During outburst, SS Cygni is the brightest CV in the sky, with an almost continuous light curve available for the last 100 years thanks to amateur astronomers. Its outburst history has been well studied and compared with disc instability predictions [5]. Phase resolved spectroscopy reveals emission from the secondary star as well as a distorted accretion disc, both in quiescence and outburst [16,17]. Doppler tomography during outburst revealed enhanced emission from the disc in the top right and lower left quadrant of the tomograms in the Balmer, HeI and HeII lines [29]. MEM maps of two emission lines are presented in Figure 11. Again, the disc has a two armed asymmetry, but on the other hand differs significantly from a simple two armed spiral pattern. SS Cyg is an intermediate inclination system, and our line of sight thus penetrates deeper into the disc atmosphere, producing broad absorption wings from the optically thick disc during outburst. This may complicate the comparison between models of spiral arms and the line emission from them because of more intricate, and poorly understood, radiative transfer conditions in the vertically stratified disc. However, these differences need an explanation and given the brightness of SS Cyg, justifies high resolution phase resolved spectroscopy of this system in quiescence and outburst.

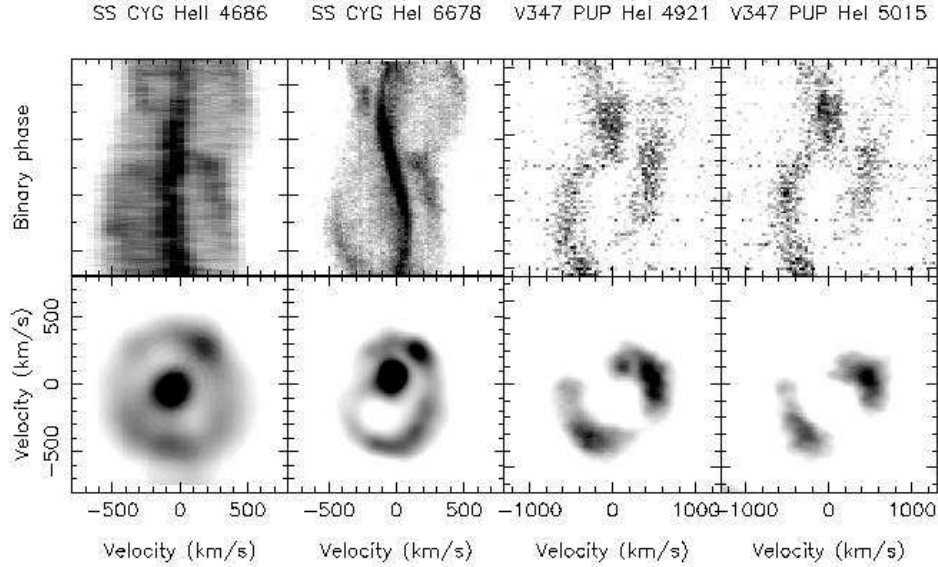


**Fig. 11.** Two other cases of distorted accretion discs with a two armed asymmetry. Left the HeII and HeI emission of SS Cygni during outburst, right two panels the eclipsing nova-like V347 Pup.

#### 5.4 V347 Pup

The accretion discs of nova-likes are in many ways regarded as dwarf nova in permanent outburst, since the high mass transfer rate in the disc keeps the disc gas ionized and stable against thermal disc instabilities. Unfortunately the properties of the emission lines of these systems remains a puzzle. The atlas of Doppler maps from [13] contains many nova-like systems, for which evidence for an accretion disc is absent in most cases. One of the few nova-likes that appears to reveal a clear signature of an accretion disc is the eclipsing nova-like V347 Pup [30]. Doppler mapping revealed the presence of an accretion disc, containing a two armed asymmetry. However, the properties of some of the emission lines at a different epoch several years later were quite different (Steeghs et al., in preparation). The Balmer lines were dominated by a spot of emission in the lower left side of the tomogram rather than the disc, a typical feature of nova-like variables. However, the HeI emission (Figure 11) appears to be originating from the disc only, and displays a two armed asymmetry like that was observed in the Balmer lines by Still et al. [30] The opportunities to investigate the tidal structures of a high mass transfer rate accretion disc are ideal in this eclipsing object, and follow up NTT data is under investigation.



### 5.5 A systematic picture?

Phase resolved spectroscopy of CVs in outburst, suitable for Doppler mapping of the accretion disc, is still limited to a small number of objects. It is very encouraging that on the occasions that such data are available and can be compared, very similar accretion disc distortions are seen. This suggests a common physical cause for these large scale asymmetries and tidally driven waves appear to offer the most likely explanation. It is interesting to note that all the dwarf novae that have indicated spiral-type distortions are long period systems above the period gap. One does expect the structure of the spiral arms to depend on the mass ratio of the binary, with higher mass ratio binaries corresponding to a heavier secondary star that induces stronger tidal torques. On the other hand selection effects work against us since the outburst of the short period systems are usually short, and suitable outburst spectroscopy of short period dwarf novae during outburst maximum is extremely rare. Tomography of OY Car in outburst [9], reveals an extended arm on the side of the gas stream impact, but not a two armed spiral pattern. Limited resolution and signal to noise in this case prevents a strong case for or against spirals in SU UMa systems.

The important question is whether spiral waves affect the structure of accretion discs under a wide range of conditions, or are merely a dynamical side effect of the expanding disc during dwarf novae outbursts. Clear progress requires a more balanced observational picture covering the observational parameter space in terms of orbital periods, mass ratios, outburst behaviour, etc. This relies on our ability to obtain a considerable number of data sets of outbursting dwarf novae, in particular during the rise and decline phases. Flexible, or even robotic, scheduling of telescope time would be highly beneficial to such projects.

Doppler tomography has proven to be an invaluable tool for the discovery and study of spiral waves in the discs of CVs. With better resolution and signal to noise data becoming available with large aperture telescopes, however, there is also room for improvements to the technique itself. In the next section I describe an extension to the Doppler tomography technique that aims to improve our ability to fit to data sets containing anisotropic emission sources, a rather common situation.

## 6 Modulation mapping

Doppler tomography provides a velocity resolved image of the accretion flow in the corotating frame of the binary. Since it relies on only a few basic assumptions, such images can be recovered in a model independent way. They then provide a perfect frame in which to compare data with models. One of those assumptions is that the flux from any point fixed in the rotating frame is constant (Marsh, this volume). However, observations show the presence of anisotropic emission sources, that modulate their emission as a function of the orbital phase. Some general examples are the irradiated front of the mass donor, the hot spot, and the anisotropic emission from spiral shocks. Doppler tomography can still be used in that case, since the Doppler map serves to present a time averaged image

of the distribution of line emission. However, one will not be able to fit the data very well, and the phase dependent information contained in the observed line profiles is lost. The remainder of this review will present a straightforward extension to the Doppler tomography method that tries to remove the above mentioned assumption from tomography.

### 6.1 Extending Doppler tomography

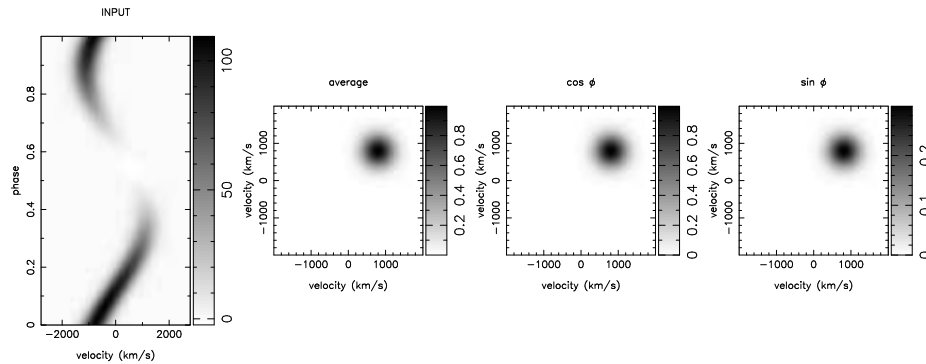


**Fig. 12.** A spot that modulates its emission across the orbital phase is not only characterised by its position in the  $V_x V_y$  plane but also the amplitude and phase of its modulation. Two additional velocity images are used to store the cosine and sine amplitudes of such S-waves. All modulations on the orbital periods can then be described as the sum of the image values in the three velocity images.

Rather than assuming that the flux from each point in the binary frame is constant, I include modulations of the flux on the orbital period. The line flux from each location (in terms of its position in the  $V_x V_y$  plane of the tomogram) is not just characterised by the average line flux, but also the amplitude and phase of any modulation on the orbital period (Figure 12). We thus have two additional parameters to describe the line flux form a specific velocity vector. The flux  $f$  from a modulated S-wave as a function of the orbital phase  $\phi$  can be written as;

$$f(\phi) = I_{avg} + I_{cos} \cos \phi + I_{sin} \sin \phi$$

where  $I_{avg}$  is the average line flux for the s-wave, and  $I_{cos}$  and  $I_{sin}$  the cosine and sine amplitudes (Figure 12). In other words, the amplitude of the modulation is  $\sqrt{I_{cos}^2 + I_{sin}^2}$ , and its phase is  $\tan^{-1}(I_{cos}/I_{sin})$ . The velocity of the S-wave is defined in terms of the vector  $V = (V_x, V_y)$  in the usual manner (Marsh, this volume);

$$v(\phi) = \gamma - V_x \cos 2\pi\phi + V_y \sin 2\pi\phi$$

With  $\gamma$  the systemic velocity of the binary. In this prescription, we need three images describing the values of  $I_{avg}, I_{cos}$  and  $I_{sin}$  for each velocity  $(V_x, V_y)$  instead of the conventional one describing  $I_{avg}$ . In other words the projection from

Doppler map to trailed spectrogram is then;

$$F(v, \phi) = \int (I_{avg}(V_x, V_y) + I_{cos}(V_x, V_y) \cos \phi + I_{sin}(V_x, V_y) \sin \phi) g(V-v) dV_x dV_y$$

with  $g(V - v)$  describing the local line profile at a Doppler shift of  $V - v$ , which is assumed to be a Gaussian convolved with the instrumental resolution.

Keith Horne implemented a similar extension to the filtered back-projection code. However, cross talk among the three terms results in significant artifacts in the back-projected maps. I choose to implement the extension using a maximum entropy optimiser in order to reconstruct artefact free images. Since the entropy is only defined for positive images, and the cosine and sine amplitudes can be either positive or negative, the problem was implemented using 5 images to characterise the data. One (positive) average image, and two (positive) images for both the cosine and sine amplitudes. For those two images one image reflects positive amplitudes, the other negative amplitudes. The image entropy for each image is defined in the usual manner relative to a running default image, and the data is fitted to a requested  $\chi^2$  while maximising the entropy of the 5 images.

## 6.2 A test reconstruction

In order to test the method, and check for possible artefacts, fake data was generated and noise was added to that data to see how well the input images can be reconstructed by the code. In Figure 13, I show an example of an input data set consisting of a constant emission from a disc as well as various anisotropic contributions from 3 spots. The large modulation of the S-waves corresponding to the spots results in a trailed spectrogram that cannot be fit using the conventional Doppler tomography technique. However, using the above described extension, the modulation mapping code is able to fit the input data to a  $\chi^2$  of 1, without introducing any spurious features in any of the images, or leaving systematic residuals to the fit. As expected, the higher the signal to noise of the input data, the more reliable and accurate the reconstruction is. Most importantly though, there is no cross-talk between the various images. A series of tests were performed to confirm that the problem is well constrained and that maximum entropy ensures that no image structure is added unless the data dictates it. Two different types of default were used. For the average image, the default is set to a Gaussian blurred version of the average image after each iteration, while for the modulation images we have tried both Gaussian blurring as well as steering the images to zero. Both converge easily to the maximum entropy solution. Of course this method suffers from the same limitations as Doppler tomography with regards to errors in the assumed systemic velocity of the binary, limited image structure due to poor signal to noise, and artefacts due to limited phase sampling.

## 6.3 Application to real data

As an example of applying the method to real data, we use the previously discussed data of SS Cygni during outburst (Figure 11). Figure 14 looks at the

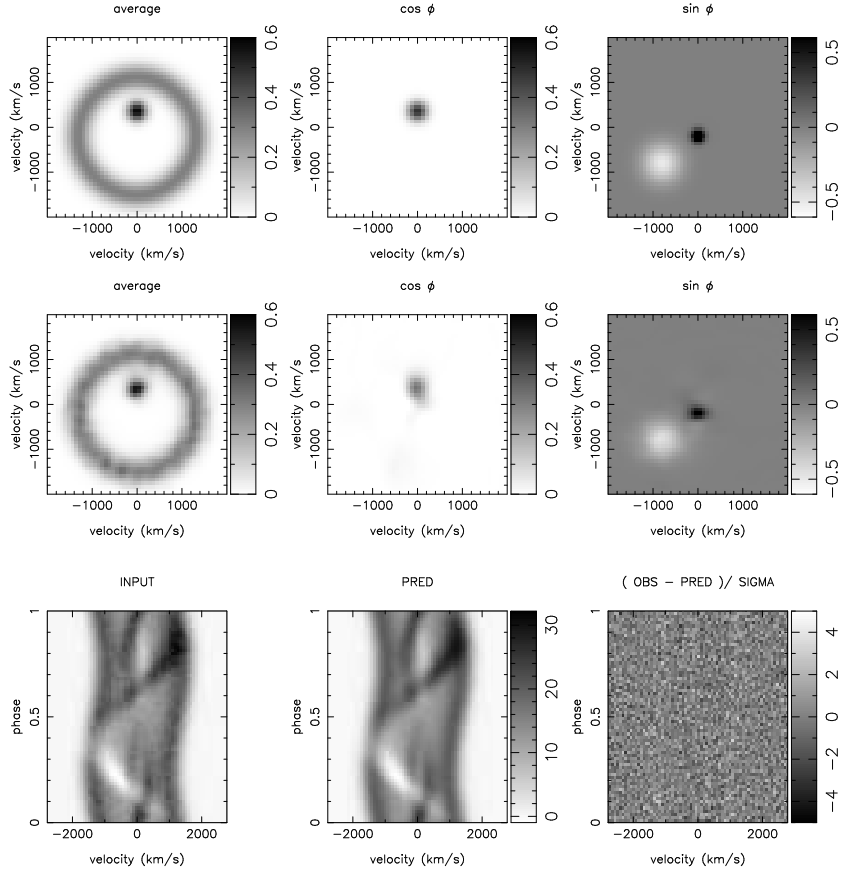


**Fig. 13.** A fake data set in order to test the reliability of modulation mapping. Top row plots the input images consisting of emission from a ring and various discrete modulated spots. The data corresponding to those images is plotted in the lower left panel (with random noise added). Middle row are the reconstructed images, bottom row compares observed and predicted data, together with a plot of the normalised residuals.

residuals between predicted and observed data when conventional MEM Doppler tomography was applied to the HeI emission line data. Although recovering the general features in the data, such as the S-wave from the irradiated secondary and the two armed disc asymmetry, residuals are significant and the best  $\chi^2$  that can be achieved is 3.2. In particular the anisotropic emission from the secondary star and parts of the disc leave large residuals due to their phase dependence. Doppler tomography tries to reproduce this phase dependence as best as it can, but is fundamentally unable to describe such emission sources adequately.

If the same data is passed to the modulation mapping code, a much better fit to the data can be obtained (Figure 15). The  $\chi^2$  value of the fit is 1, as good as one may expect, and leaves much reduced residuals between data and fit.

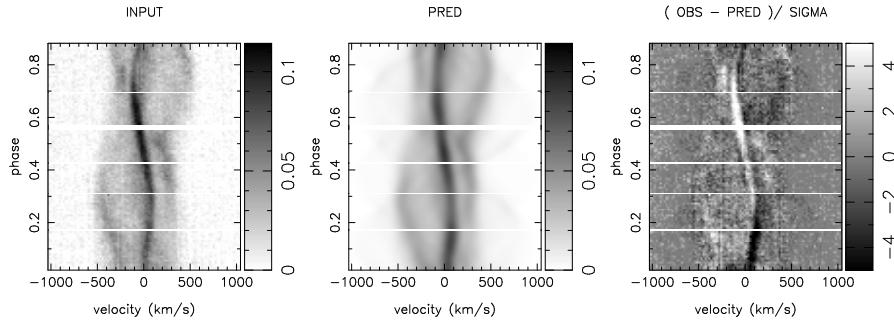


**Fig. 14.** The result of Doppler tomography of SS Cyg in outburst. The observed trailed spectrogram of HeI6678 is on the left, the predicted data of the reconstructed tomogram in the middle panel. The tomogram itself was shown in Figure 11. Significant residuals (right panel) exist due to the anisotropic emission from the secondary star and parts of the disc.

The structure of the average image is very similar to that obtained with the conventional method, indicating that the majority of the emission is relatively unmodulated. In the two modulated images, one can identify in particular the emission from the secondary and some areas of the disc. However, the two images tell us not only where the modulated emission is coming from, but also the phase of the modulation. The secondary star emission shows a left-right asymmetry in the cosine image, and a front-back asymmetry in the sine image, indicating that the emission is indeed beamed away from the Roche lobe surface. Although one ideally applies Roche tomography in order to model the contribution of the secondary, modulation mapping ensures that strong anisotropic S-waves originating from the mass donor are fitted well, and that they do not leave artefacts or limit the goodness of fit that can be achieved.

Obvious other emission sources where the phasing and beaming of the emission can be quantified with this method are the emission from the bright spot, and emission from anisotropic spiral shocks. In SS Cygni, the emission from the disc seems to be only weakly modulated (Figure 16), which may not be too surprising because of its low orbital inclination  $i$ . Shear broadening, for example, leads to anisotropic emission and is proportional to  $\cos^{-1} i$ . Its effect is thus considerably reduced for inclinations below  $60^\circ$  [26]. Work is in progress to apply this method to the emission of the spirals in IP Peg and other objects in order to quantify the anisotropy of the emission from the spiral shocks.

Modulation mapping provides a straightforward extension to Doppler tomography, with a wide range of applications. The code as such does not need to make any assumptions about the nature of the modulations, except that the period of modulation is the orbital period. It thus relaxes one of the fundamental assumption of Doppler tomography, in order to make the technique more versatile. Many data sets already exist that could benefit from this extension, but it will be of particular use for the high resolution data sets that will be obtained with

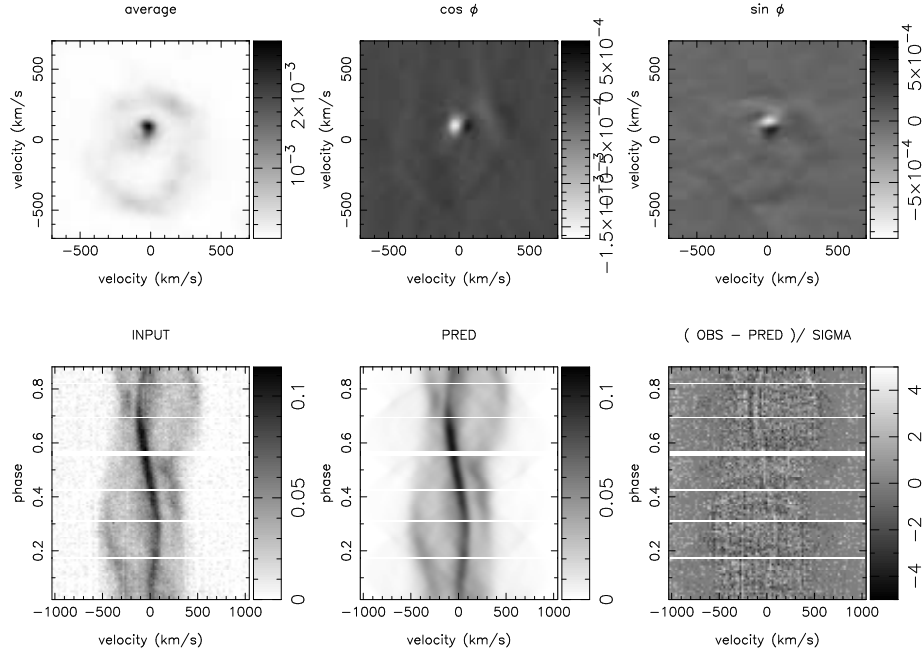


**Fig. 15.** The same SS Cygni data now processed with the modulation mapping code. Top row are the reconstructed images, with the observed and predicted spectrogram in the bottom row.

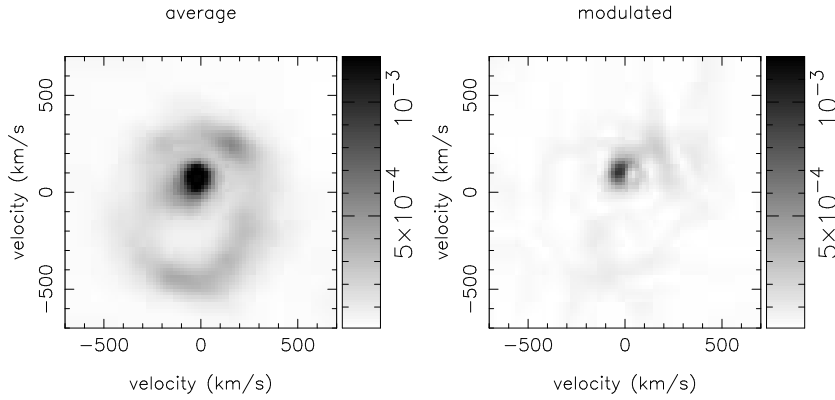


**Fig. 16.** A closer look at the derived tomograms with modulation mapping. Left the average image, right the total amplitude in the modulated images. Most prominent is the modulated emission from the secondary star, as well as a small contribution from the disc.

the new large aperture telescopes. An even more general prescription can easily be envisaged that attempts to model modulations on other periods as well.

## 7 Conclusions

Doppler tomography of the dwarf nova IP Peg has revealed a remarkable two armed spiral structure in its accretion disc that dominates the emission from a range of emission lines over a large range of radii. The pattern is observed from the start of the outburst up to the later stages of the outburst maximum, and is fixed in the binary frame. Its location in the tomograms fits remarkably well with the two armed spiral shocks that are expected to be generated by the tidal torques of the companion star. A tidal origin is also supported by the fact that the structure is corotating with the binary for at least 50 orbital periods, and the fact that the asymmetry is not visible during quiescence, when tidal torques on the much smaller accretion disc are significantly reduced.

In order to appreciate the relevance of tidally driven spiral waves for the structure of accretion discs in general, a more varied observational picture is required, spanning a range of objects and source states. Since the detection of spirals in IP Pegasi, a handful of other systems have displayed very similar disc structures, but a systematic picture is still difficult to extract. A second important restriction of the current data sets, is the limited coverage we have of each outburst. In the CV sub-class of dwarf novae we have a truly unique opportunity to track the evolution of the disc in real-time through time-lapsed tomography. What is needed is a focused campaign that aims to obtain spectroscopy across a significant fraction of the outburst cycle. Such a data set would be an extremely valuable test bed for both disc instability models as well as the question of angular momentum transport associated with density waves. Although the observed spirals appear to fit to detailed simulation in surprising detail, it is still not clear what the impact of such prominent spiral arms is on the angular momentum budget of the disc and how it relates to the local shear viscosity. This requires improved observations and realistic simulations in order to test quantitatively the impact of such waves (Boffin, this volume).

I also discussed an extension to Doppler tomography, with the aim of mapping modulated emission sources in emission line data. This is a rather common situation and will not only benefit the observational study of spiral waves, but a range of other emission sources commonly observed. I demonstrated that artefact free reconstructions can be calculated from phase resolved spectroscopy using maximum entropy regularisation.

## References

1. Balbus S. A., Hawley J. F., 1991, *ApJ*, 376, 214
2. Baptista R., Harlaftis E. T., Steeghs D., 2000, *MNRAS*, 314, 727
3. Billington I., Marsh T.R., Dhillon V.S., 1996, *MNRAS*, 278, 673

4. Binney J., Tremaine S., 1987, *Galactic Dynamics*. Princeton Series in Astrophysics, Princeton University Press
5. Cannizzo, J. K., Mattei, J. A., 1998, *ApJ*, 505, 344
6. Fiedler H., Barwig H., Mantel K. H., 1997, *A&A*, 327, 173
7. Frank J., King A., Raine D., 1985, *Accretion Power in Astrophysics*, Cambridge Astrophysics Series, Cambridge University Press
8. Groot P., 2000, *ApJL*, submitted
9. Harlaftis, E.T, Marsh, T., 1996, *A&A*, 308, 97
10. Harlaftis E. T., Marsh T. R., Dhillon V. S., Charles P. A., 1994, *MNRAS*, 267, 473
11. Harlaftis E. T., Steeghs D., Horne K., Martin E., T. M., 1999, *MNRAS*
12. Joergens V., Spruit H. C., Rutten R. G. M., 2000, *A&A*, 356, 33
13. Kaitchuck R. H., Schlegel E. M., Honeycutt R. K., Horne K., Marsh T. R., White J. C. I., Mansperger C. S., 1994, *ApJS*, 93, 519
14. Livio M., 1994, in "Interacting Binaries", Saas-Fee Advanced Course 22. Lecture Notes 1992. Swiss Society for Astrophysics and Astronomy, XVI, Springer-Verlag Berlin Heidelberg New York
15. Marsh T. R., Horne K., 1990, *ApJ*, 349, 593
16. Martinez-Pais I. G., Giovannelli F., Rossi C., Gaudenzi S., 1994, *A&A*, 291, 455
17. Martinez-Pais I. G., Giovannelli F., Rossi C., Gaudenzi S., 1996, *A&A*, 308, 833
18. Morales-Rueda L., Marsh T., Billington I., 1999, *MNRAS*,
19. Pringle J. E., 1981, *ARA&A*, 19, 137
20. Savonije G.J., Papaloizou J.C.B., Lin D.N.C., 1994, *MNRAS*, 268, 13
21. Sawada K., Matsuda T., Hachisu I., 1986, *MNRAS*, 219, 75
22. Shakura N. I., Sunyaev R. A., 1973, *A&A*, 24, 337
23. Spruit H. C., Matsuda T., Inoue M., Sawada K., 1987, *MNRAS*, 229, 517
24. Spruit H. C., 1987, *A&A*, 184, 173
25. Steeghs D., 1999, PhD thesis, University of St.Andrews (available at <http://www.astro.soton.ac.uk/~ds/thesis.html>).
26. Steeghs D., Stehle R., 1999, *MNRAS*, 307, 99
27. Steeghs D., Harlaftis E. T., Horne K., 1997, *MNRAS*, 290, L28
28. Steeghs D., Harlaftis E. T., Horne K., 1998, *MNRAS*, 296, 463
29. Steeghs D., Horne K., Marsh T. R., Donati J. F., 1996, *MNRAS*, 281, 626
30. Still M. D., Buckley D. A. H., Garlick M. A., 1998, *MNRAS*, 299, 545
31. Toomre A., 1969, *ApJ*, 158, 899
32. Wolf S., Mantel K. H., Horne K., Barwig H., Schoembs R., Baernbantner O., 1993, *A&A*, 273, 160
33. Wolf S., Barwig H., Bobinger A., Mantel K.-H., Simic D., 1998, *A&A*, 332, 984
34. Wood J., Horne K., Berriman G., Wade R., O'Donoghue D., Warner B., 1986, *MNRAS*, 219, 629